Monthly Notices
of the
ROYAL ASTRONOMICAL SOCIETY

MNRAS **477,** 5115–5126 (2018)
Advance Access publication 2018 April 17

doi:10.1093/mnras/sty901

Extreme gaseous outflows in radio-loud narrow-line Seyfert 1 galaxies

S. Komossa,[1]★ D. W. Xu[2,3,4] and A. Y. Wagner[5,6]

[1]*Max-Planck-Institut für Radioastronomie, Auf dem Hügel 69, D-53121 Bonn, Germany*
[2]*Key Laboratory of Space Astronomy and Technology, National Astronomical Observatories, Chinese Academy of Science, 20A Datun Road, Chaoyang District, Beijing 100012, China*
[3]*National Astronomical Observatories, Chinese Academy of Science, 20A Datun Road, Chaoyang District, Beijing 100012, China*
[4]*School of Astronomy and Space Sience, University of the Chinese Academy of Sciences, 19A Yuquan Road, Shijingshan District, Beijing 100049, China*
[5]*Center for Computational Sciences, University of Tsukuba, 1-1-1 Tennodai, Tsukuba, Ibaraki 305-8577, Japan*
[6]*Institut d'Astrophysique de Paris, 98 bis bd Arago, F-75014 Paris, France*

Accepted 2018 April 7. Received 2018 April 1; in original form 2018 February 15

ABSTRACT

We present four radio-loud narrow-line Seyfert 1 (NLS1) galaxies with extreme emission-line shifts, indicating radial outflow velocities of the ionized gas of up to 2450 km s^{-1}, above the escape velocity of the host galaxies. The forbidden lines show strong broadening, up to 2270 km s^{-1}. An ionization stratification (higher line shift at higher ionization potential) implies that we see a large-scale outflow rather than single, localized jet–cloud interactions. Similarly, the paucity of zero-velocity [O III] λ5007 emitting gas implies the absence of a second narrow-line region (NLR) component at rest, and therefore a large part of the high-ionization NLR is affected by the outflow. Given the radio loudness of these NLS1 galaxies, the observations are consistent with a pole on view onto their central engines, so that the effects of polar outflows are maximized. In addition, a very efficient driving mechanism is required to reach the high observed velocities. We explore implications from recent hydrodynamic simulations of the interaction between fast winds or jets with the large-scale NLR. Overall, the best agreement with observations (and especially the high outflow speeds of the [Ne V] emitting gas) can be reached if the NLS1 galaxies are relatively young sources with lifetimes not much exceeding 1 Myr. These systems represent sites of strong feedback at NLR scales at work, well below redshift one.

Key words: galaxies: active – galaxies: evolution – galaxies: individual: SDSSJ130522.75+511640.3, SDSSJ144318.56+472556.7, SDSSJ150506.48+032630.8, SDSSJ163401.94+480940.2 – galaxies: jets – quasars: emission lines – galaxies: Seyfert.

1 INTRODUCTION

Powerful gaseous outflows in active galactic nuclei (AGNs) deposit mass, energy, and metals in the interstellar medium of the host galaxy or on even larger scales (e.g. Colbert et al. 1996; Churazov et al. 2001; Moll et al. 2007; Hopkins et al. 2016). They therefore shape the structure and composition of the AGN environment and may play an important role in unified models (e.g. Elvis 2006).

The most powerful of these outflows can significantly affect the co-evolution of galaxies and black holes by feedback processes (e.g. Fabian 1999; Wyithe & Loeb 2003), especially by regulating star formation, and possibly clearing the host galaxy of large fractions of its inhomogeneous interstellar medium (ISM; e.g. di Matteo, Springel & Hernquist 2005; Springel, Di Matteo & Hernquist 2005; Hopkins & Elvis 2010; Zubovas & King 2012; Hopkins et al. 2016).

There is ample observational evidence for mild winds and outflows in AGN (e.g. Crenshaw & Kraemer 2007; Fabian 2012). In the optical and IR regime, they manifest as emission-line shifts and line asymmetries. Narrow emission lines in nearby AGN typically imply outflow velocities of less than a few 100 km s^{-1} in the high-ionization gas, even though much higher values have occasionally been reported, especially seen in 'blue wings' of the [O III] λ5007 emission line (e.g. Capetti et al. 1999; Holt, Tadhunter & Morganti 2003; Das et al. 2005; Das et al. 2006; Holt, Tadhunter & Morganti 2008; Kraemer et al. 2009; Mazzalay et al. 2010; Nesvadba et al. 2011; Villar-Martin et al. 2011; Jin, Ward & Done 2012; Bae & Woo 2014; Komossa et al. 2015; Shen 2016; Woo et al. 2016; Perna et al. 2017; Wang, Xu & Wei 2018). Most of these do not affect the whole narrow-line region (NLR), but occur in localized regions, sometimes though not always spatially coincident with radio jets. Long-slit and integral field spectroscopy have been powerful tools in uncovering them. In other instances, the outflows are widely extended, and/or involve the whole [O III] emission (e.g.

★ E-mail: stefanie.komossa@gmx.de

Table 1. Galaxy radio properties.

Coordinates (1)[a]	Abbreviated name (2)	z (3)	log R (4)	$f_{0.15\,\mathrm{GHz}}$ (5)	$f_{1.4\,\mathrm{GHz}}$ (6)	$f_{4.85\,\mathrm{GHz}}$ (7)	$f_{22\,\mathrm{GHz}}$ (8)	α_r (9)
13:05:22.75+51:16:40.3	SDSSJ1305+5116	0.785	2.34	320	87/87	46	<9	−0.51
14:43:18.56+47:25:56.7	SDSSJ1443+4725	0.703	3.07	359	171/166	59	<16	−0.86
15:05:06.48+03:26:30.8	SDSSJ1505+0326	0.409	3.19	120	380/395	991	697	0.77
16:34:01.94+48:09:40.2	SDSSJ1634+4809	0.495	2.31	–	8/14	–	–	–

[a]Columns from left to right: (1) SDSS optical J2000 coordinates in RA (h,m,s) and DEC (d,m,s); (2) galaxy name used in this work; (3) SDSS redshift; (4) radio-loudness index R (Kellermann et al. 1989) defined as f_ν(1.4 GHz)/f_ν(4400Å) from Yuan et al. (2008); (5)–(8) radio flux densities in mJy at 151 MHz, 1.4 (FIRST/NVSS), 4.85 and 22 GHz collected from the literature (Condon et al. 1998; Gregory & Condon 1991; Hales et al. 2007; Helfand et al. 2015; Doi et al. 2016); (9) spectral slope α_r between 1.4 GHz (FIRST) and 4.85 GHz, based on non-simultaneous data.

Zamanov et al. 2002; Marziani et al. 2003; Boroson 2005; Komossa et al. 2008; Zhang et al. 2011; Bae & Woo 2014; Harrison et al. 2014; Berton et al. 2016; Cracco et al. 2016; Marziani et al. 2016; Zakamska et al. 2016; Rupke et al. 2017). Galaxies which show a systematic shift of their whole [O III] emission line with respect to Hβ have been termed 'blue outliers' (Zamanov et al. 2002). All galaxies of our study are blue outliers.

The driving force of these outflows has remained unclear. Accretion-disc winds, radiation pressure acting on dusty gas, entrainment of gas in radio plasma, and variants thereof, have all been considered (e.g. Murray et al. 1995; Binette 1998; Proga et al. 2000; Saxton et al. 2005; Proga, Ostriker & Kurosawa 2008; Wagner, Bicknell & Umemura 2012; Wagner, Umemura & Bicknell 2013; Thompson et al. 2015; Bieri et al. 2017; Cielo et al. 2018; Costa et al. 2018).

There are indications that winds are especially strong in NLS1 galaxies, where accretion near the Eddington limit likely triggers strong, radiation pressure-driven outflows (e.g. Boroson 2002; Grupe 2004; Grupe et al. 2010; Xu et al. 2012). NLS1 galaxies are a subclass of AGN with extreme multiwavelength properties. Common definition criteria are small widths of their broad Balmer lines of FWHM(Hβ) $< 2000\,\mathrm{km\,s^{-1}}$, faint emission of [O III]/Hβ < 3, and strong Fe II emission complexes (Osterbrock & Pogge 1985; Goodrich 1989; Véron-Cetty, Véron & Goncalves 2001). About 16 per cent of all NLS1 galaxies are blue outliers and exhibit strong kinematic shifts of their [O III] emission-line cores ($v > 150\,\mathrm{km\,s^{-1}}$, Komossa et al. 2008).

While NLS1 galaxies are on average more radio-quiet than broad-line AGN (Komossa et al. 2006), a small fraction of them is beamed and radio loud (Komossa et al. 2006; Yuan et al. 2008), highly variable at radio frequencies (Abdo et al. 2009c; Lähteenmäki et al. 2017), and detected at γ-rays (Abdo et al. 2009a,b, Foschini 2011; D'Ammando et al. 2012, 2015; Yao et al. 2015; Paliya et al. 2018; Yang et al. 2018).

If radio loudness of NLS1 galaxies is generally due to beaming, we expect a pole on view onto these galaxies, and so the effects of (polar) outflows are maximized. We have analysed four radio-loud NLS1 galaxies of the sample of Yuan et al. (2008), which were initially noted for their shifted [O III] emission lines, placing them in the class of blue outliers. We show that all four galaxies of our study exhibit extreme line shifts, among the highest measured so far. They therefore provide us with powerful tools of understanding extreme gaseous outflows in NLS1 galaxies; their drivers, possible association with radio jets, and their impact on the environment. This is the first dedicated study of highly ionized gas outflows in the radio-loudest NLS1 galaxies including emission lines other than the [O III] λ5007–Hβ complex. First results were reported by Komossa et al. (2016).

This paper is organized as follows. In Section 2, we describe the methods of data analysis and present the results. Notes on individual galaxies are given in Section 3. We then confront the large measured emission-line shifts and widths with different outflow mechanisms (Section 4). Conclusions are provided in Section 5. We use a cosmology (Wright 2006) with $H_0 = 70\,\mathrm{km\,s^{-1}\,Mpc^{-1}}$, $\Omega_\mathrm{M} = 0.3$, and $\Omega_\Lambda = 0.7$ throughout this paper.

Finally, we would like to emphasize that [O III] line shifts come in two types, and we keep this distinction throughout this paper: The [O III] emission line can typically be fit by *two* Gaussian components; one strong prime component which we refer to as narrow 'core component' of the emission line, and a second, fainter and broader component which is often shifted towards the blue w.r.t. the core component, and is commonly referred to as blue wing. Many studies of [O III] outflows are based on just these blue wings, while in blue outliers (including those discussed here), the *whole core profile* of [O III] is shifted. Blue wings are additionally present in our sources and show extreme shifts and widths.

2 DATA ANALYSIS AND RESULTS

2.1 Data preparation

The four galaxies (Table 1) have been observed in the course of the Sloan Digital Sky Survey (SDSS; York et al. 2000; Zhou et al. 2006; Schneider et al. 2007; Shen et al. 2011), and we have retrieved the spectra from data release DR7 (Abazajian et al. 2009) for analysis. The data preparation and spectral analysis has been performed in a standard way, similar to Xu et al. (2007). The spectra were corrected for Galactic extinction, according to Schlegel et al. (1998). All spectra show strong emission complexes from Fe II in the optical and ultraviolet (UV), and therefore Fe II templates were prepared and subtracted before further emission-line analysis. In the optical, the Fe II template of Véron-Cetty, Joly & Véron (2004) was used, while in the UV we employed the template of Bruhweiler & Verner (2008). It was assumed that Fe II has the same profile as the broad component of Hβ. When we report measurements of optical Fe II strength, Fe II λ4570, this is the integrated flux of the Fe II emission complex between the rest wavelengths 4434 Å and 4684 Å. R4570 corresponds to the ratio Fe II λ4570/Hβ. Some basic properties of the four galaxies are listed in Table 1, including source redshift and radio properties collected from the literature.

2.2 Emission-line fits

The spectra (Fig. 1) show emission lines from Hβ, [O II] λ3727, [O III] λλ5007,4959, [Ne III] λ3869, [Ne V] λ3426, Mg II λ2798, and C II] λ2325. SDSSJ1305+5116 and SDSSJ1443+4725 further show

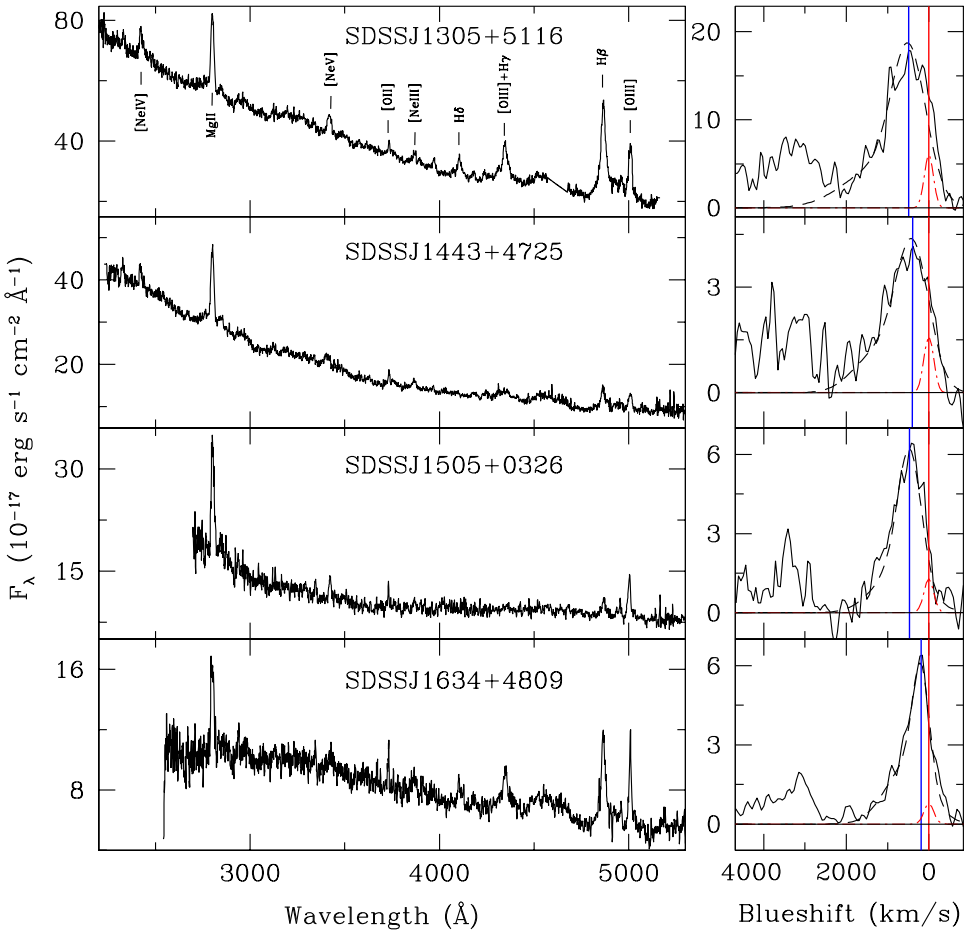

Figure 1. Left-hand panel: SDSS spectra of the four radio-loud NLS1 galaxies (rest-frame wavelength based on SDSS redshift). Right-hand panel: zoom on the [O III] λλ4959,5007 emission-line doublet of the four galaxies, after subtraction of Fe II emission and continuum. The [O III] line blueshift is measured with respect to [O II]. The red dotted line marks the maximum contribution of a Gaussian with zero blueshift. The solid blue line marks the line peak location based on Gaussian fitting. See the electronic edition of the Journal for a colour version of this figure.

a line near 2424 Å; likely due to [Ne IV] with a possible contribution from Fe III (Section 2.8). Emission line fits were carried out with the IRAF package SPECFIT (Kriss 1994). Emission lines were fit with Gaussian profiles, in a way similar to Komossa et al. (2008; K08 hereafter), which also allows easy comparison with that sample of NLS1 galaxies and blue outliers in particular. The one difference with the blue outliers of K08 is the higher redshifts of the four galaxies analysed here, and so the [S II] λλ6716,6731 lines used previously for reference when measuring kinematic shifts are no longer observable. Instead, we have therefore measured line shifts with respect to [O II] λ3727.

Emission-line shifts, FWHMs (full width at half-maximum), and fluxes were measured. Results are reported in Table 2. All FWHMs given in this paper have been corrected for instrumental broadening. Most emission lines are well represented by a single Gaussian profile. Exceptions are the brightest emission lines, [O III], Hβ, and MgII. Hβ was decomposed into three components: a narrow component ($H\beta_n$) and two broad components. No physical meaning is ascribed to the two separate broad components; they merely serve as a mathematical description (a Lorentzian often is an alternative to describe such profiles; e.g. Véron-Cetty et al. 2001; Sulentic et al. 2002). The final width of the broad-line emission, $H\beta_b$, reported in Table 2 and throughout this paper, is then determined as the FWHM of the sum of those two Gaussians.

The total [O III] emission-line profile, $[O\,III]_{totl}$, was decomposed into two Gaussian components, a narrow core ($[O\,III]_c$) and a broad 'wing' component ($[O\,III]_w$). Measurements of the FWHM and blueshift of [O III] reported in this work refer to the core of the emission line, unless noted otherwise. Mg II was fit with two Gaussian components, a narrow and a broad component. Results are reported in Table 2. The optical spectra of all four galaxies are shown in Fig. 1, while a zoom on the [Ne V] emission of the two galaxies with the highest outflow velocities is given in Fig. 2.

2.3 Limits on the presence of a zero-velocity [O III] component and of highly blueshifted Hβ

We have used the spectrum of SDSSJ1305+5116, the brightest of the four sources, for some further measurements. First, we have checked for the presence of an Hβ 'counterpart' to the blueshifted [OIII] core component. We did so by refitting the Hβ profile with an extra Gaussian, its FWHM and peak shift fixed to that of [OIII]. The two remaining broad (and the narrow) Gaussians were left free to vary. This procedure allows us to estimate the maximum emission from any highly blueshifted Hβ, if any, consistent with the spectrum. We find that the presence of blueshifted Hβ is consistent with the spectrum of SDSSJ1305+5116, with a maximum contribution of 15 per cent in flux.

Table 2. Emission-line measurements.

Galaxy name/ line (1)[a]	Δv (2)	f (3)	FWHM (4)
SDSSJ1305+5116			
Mg II$_n$	460	0.17	500
Mg II$_b$	400	9.37	2170
C II]	− 50	1.23	1220
[Ne IV][b]	660	2.66	1710
[Ne V]	1360	3.71	2300
[O II]	0	0.70	650
[Ne III]	640	1.19	1190
[O III]$_c$	480	4.85	950
[O III]$_w$	1230	2.71	1950
Hβ_n	150	0.49	500
Hβ_b	270	22.6	1990
R4570		0.62	
SDSSJ1443+4725			
Mg II$_n$	230	0.10	200
Mg II$_b$	250	7.01	2300
C II]	220	0.72	950
[Ne IV] [b]	750	0.99	1100
[Ne V]	2450	1.67	2270
[O II]	0	0.35	490
[Ne III]	760	0.62	1140
[O III]$_c$	400	1.18	940
[O III]$_w$	1280	0.42	1300
Hβ_n	420	0.20	290
Hβ_b	340	2.79	1700
R4570		2.2	
SDSSJ1505+0326			
Mg II$_n$	170	0.05	260
Mg II$_b$	170	3.73	1500
[Ne V]	680	0.68	1070
[O II]	0	0.23	270
[O III]$_c$	460	0.78	640
[O III]$_w$	720	0.57	1390
Hβ_n	− 80	0.05	250
Hβ_b	− 110	0.84	1440
R4570		1.63	
SDSSJ1634+4809			
Mg II$_n$	90	0.05	400
Mg II$_b$	90	1.54	1840
[Ne V]	520	0.20	1270
[O II]	0	0.20	400
[Ne III]	460	0.32	1140
[O III]$_c$	190	0.55	450
[O III]$_w$	520	0.72	1220
Hβ_n	80	0.21	370
Hβ_b	10	3.61	1770
R4570		1.02	

[a]Columns from left to right: (1) emission line; (2) emission-line inflow (negative sign) or outflow velocity, measured relative to [OII], in km s^{-1}; (3) measured line flux, in 10^{-15} erg cm^{-2} s^{-1}; (4) line width (FWHM), corrected for instrumental broadening, in km s^{-1}.
[b]Line identification uncertain. See Section 2.8 for details.

Second, in order to see, how much zero-velocity [O III] emitting gas there is, we have also fit an extra Gaussian to [O III] fixed at a narrow width of only FWHM = 230 km s^{-1} (the average width of low-ionization emission lines in the sample of K08), and at the same redshift as [O II]. We find little if any contribution of zero-velocity [O III], with an upper limit of typically 1–5 per cent of the total flux in [O III].

Finally, the broad Balmer-line component, Hβ_b, was inspected for a possible blueshift. In our fitting procedure, the broad part

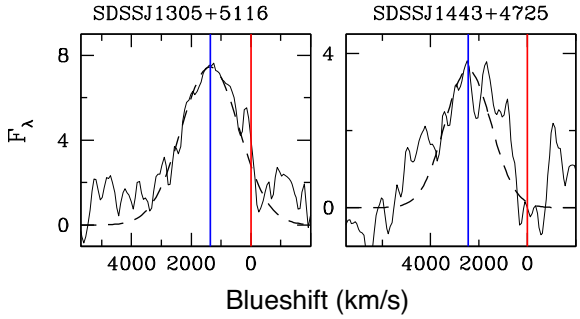

Figure 2. Observed [Ne V] λ3426 line profile of the two galaxies with the highest outflow velocities and fitted Gaussian profile.

of the emission line was approximated by two Gaussian components. On average, these do not show significant blue or redshifts beyond ∼300 km s^{-1}, and always remain below the high shifts seen in the high-ionization emission lines. Therefore, the bulk of the Hβ-emitting broad-line region (BLR) does not participate in the high-velocity outflow.

2.4 Measurement uncertainties

In order to see, how much the measurement of the narrow emission line parameters are affected by emission-line decomposition and by the way the continuum is modelled, we have performed various tests, including different ways of measuring line widths and peak shifts, and fitting only a fraction of the full profile. We find that uncertainties in line widths and shifts are typically within 10–20 per cent.

The NLS1 galaxies of our study are also included in a number of large SDSS NLS1/quasar catalogues, which also list Hβ line fits. We have compared our fit results with those previous reports and find overall good agreement, given the fact that (1) those previous studies were standardized line fittings for very large samples and (2) different line decompositions were employed including (i) Lorentzian fits with or without adding a narrow-line component or (ii) multiple Gaussian fits (one to three components) with or without including a NLR component. For instance, for SDSSJ1305+5116, Zhou et al. (2006) reported FWHM(Hβ) = 1952 km s^{-1}, which compares to 1963 km s^{-1} of Rakshit et al. (2017) and 1990 km s^{-1} (our Table 3). Berton et al. (2016) analysed the [O III] profile of a sample of NLS1 galaxies. While they determined FWHM([O III]$_c$) = 1012 km s^{-1} for SDSSJ1305+5116, we derived 950 km s^{-1}.

2.5 NLS1 classification

We have always used Gaussians to fit Hβ. We confirm the NLS1 classification (Zhou et al. 2006) of all four galaxies, since always FWHM(Hβ_b) < 2000 km s^{-1}. However, it is interesting to note that the *broadest* component of Hβ (we recall that we fit each Hβ with two broad components, and the FWHM represents the sum of those two) of SDSSJ1634+4809 is relatively broad, with FWHM(Hβ_{b2}) = 4960 km s^{-1}. This reflects the fact that AGN with narrow broad lines are often well fit with Lorentzian profiles (e.g. Véron-Cetty et al. 2001; Sulentic et al. 2002).

2.6 Extreme velocities and line widths

Extreme emission-line blueshifts are present in all four spectra. In [O III], SDSSJ1305+5116 and SDSSJ1505+0326 show the

Table 3. Galaxy properties.

Name (1)[a]	log L_{bol} (2)	log $M_{BH,H\beta}$ (3)	L/L_{Edd} (4)	log $M_{BH,Mg\,II}$ (5)	P_{jet} (6)	η_{jet} (7)	M_{out} (8)
SDSSJ1305+5116	46.5	8.4	0.95	8.1	5.0	0.015	8.7
SDSSJ1443+4725	45.6	7.6	0.79	7.9	6.1	0.11	1.6
SDSSJ1505+0326	44.7	6.8	0.66	7.0	4.3	0.52	0.3
SDSSJ1634+4809	45.4	7.5	0.65	7.1	1.4	0.03	0.3

[a]Columns from left to right: (1) galaxy name, (2) bolometric luminosity, (3) Hβ-based SMBH mass in solar masses, (4) Eddington ratio, (5) MgII-based SMBH mass in solar masses, (6) jet power in 10^{44} erg s^{-1}, (7) jet Eddington ratio, (8) ionized gas mass in outflow, in 10^7 M$_\odot$.

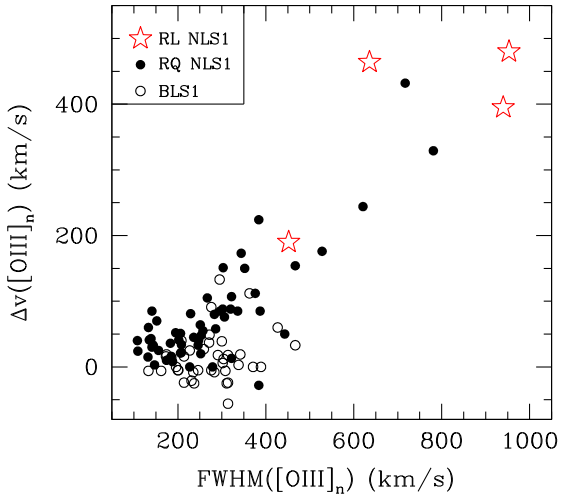

Figure 3. Shift-width correlation of the core of [O III] λ5007. For comparison, the sample of BLS1 galaxies (open circles) and NLS1 galaxies (filled circles) of Komossa et al. (2008) is plotted.

highest, with FWHM([O III]$_c$) = 950 km s^{-1} and Δv([O III]$_c$) = 480 km s^{-1} (SDSSJ1305+5116) and FWHM([O III]$_c$) = 640 km s^{-1} and Δv([O III]$_c$) = 460 km s^{-1} (SDSSJ1505+0326). Blue wings in [O III] are additionally present, and these show even higher shifts and widths; reaching FWHM([O III]$_w$) = 1950 km s^{-1} and Δv([O III]$_w$) = 1230 km s^{-1} in the case of SDSSJ1305+5116.

High-ionization lines of [Ne V] are identified in all spectra. The highest measured shifts are Δv([Ne V]) = 2450 km s^{-1} (SDSSJ1443+4725) and Δv([Ne V]) = 1360 km s^{-1} (SDSSJ1305+5116).

The [O III] emission lines follow a width-shift correlation, in the sense that more highly shifted lines are much broader (Fig. 3), similar to the trend seen in radio-quiet NLS1 galaxies and higher-redshift quasars. The same pattern is followed by [Ne V]. Such a trend can be reproduced, if outflows of higher velocity come with larger outflow-cone opening angles (Bae & Woo 2016), or with higher gas turbulence. Since in these cases, the emission-line width does not reflect the host bulge potential, FWHM([O III]) is not a good surrogate for stellar velocity dispersion (Komossa & Xu 2007), and therefore cannot be used for independent BH mass estimates (Section 2.9) of these radio-loud NLS1 galaxies.

2.7 A correlation of line shift with ionization potential

The higher-ionization lines show the higher blueshifts. We have therefore plotted in Fig. 4 the dependence of radial velocity Δv on ionization potential IP of each respective ion, in comparison to our previous sample of blue outliers (K08). Despite some scatter in the low-ionization lines, and especially Mg II, there is an overall trend of higher blueshift with higher ionization potential.[1]

Fig. 5 shows the dependence on critical density. By chance, higher ionization potentials of the ions discussed here also generally come with higher critical densities of the forbidden line transitions observed from the respective ions. Therefore, a correlation between outflow velocity and ionization potential generally implies a correlation with critical density, and vice versa, raising the question which of the two is the fundamental one: density stratification or ionization stratification. An important exception to the above rule is [O I] λ6300. Its critical density (n_{crit} = 1.8 10^6 cm^{-3}) is relatively high, while its ionization potential is zero. Unfortunately, [O I] is not observed in the four radio-loud NLS1 galaxies because of their high redshift. If the same driver of the outflow is at work as in the radio-quiet NLS1 galaxies, then the deviation of [O I] (Fig. 5) suggests that the trend with IP is the more fundamental one.

2.8 Identification of the line near 2424 Å

The spectra of SDSSJ1305+5116 and SDSSJ1443+4725 show an emission line at a rest wavelength of λ_o = 2422.1 Å and 2420.8 Å, respectively. This feature is near the location of [Ne IV], which has been previously identified in the SDSS spectra of AGN, at a laboratory wavelength of 2424 Å (table 2 of vanden Berk et al. 2001). If we do identify the observed feature in the spectra of SDSSJ1305+5116 and SDSSJ1443+4725 with [Ne IV], then outflow velocities of Δv(Ne IV) = 660 km s^{-1} and 750 km s^{-1} (SDSSJ1305+5116 and SDSSJ1443+4725, respectively) are inferred. Given the possibility of a blend with Fe III transitions (vanden Berk et al. 2001), we do not include [Ne IV] in the figures. We do list it in Table 2, and line parameters in that table have been inferred under the assumption that we indeed see [Ne IV].

2.9 Black hole masses and Eddington ratios

Supermassive black hole (SMBH) masses were estimated based on the virial relation established for broad-line AGN, using the line width of Hβ_b. Since the optical continuum luminosity is likely dominated by the jet emission, we make use of the Hβ line luminosity instead (Vestergaard & Peterson 2006):

$$M_{BH} = 10^{6.67} \left(\frac{L_{H\beta}}{10^{42}\ \mathrm{erg\ s^{-1}}} \right)^{0.63} \left(\frac{\mathrm{FWHM(H}\beta)}{1000\ \mathrm{km\ s^{-1}}} \right)^{2} \mathrm{M}_\odot. \quad (1)$$

This gives SMBH masses in the range ($6 \times 10^6 - 3 \times 10^8$) M$_\odot$ (Table 3).

[1]Note the tendency in several (but not all) nearby Seyfert galaxies that high-ionization lines are typically more blueshifted than low-ionization lines (e.g. Penston et al. 1984; De Robertis & Osterbrock 1984; fig. 2 of Kraemer & Crenshaw 2000; fig. 17 of Mazzalay et al. 2010).

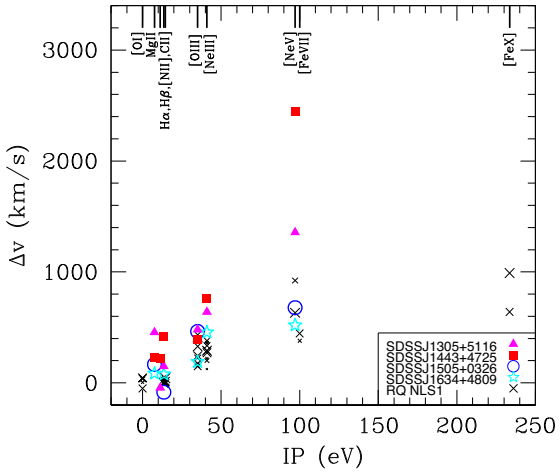

Figure 4. Radial velocity as a function of ionization potential IP. The four galaxies of this study are marked by large red and blue symbols. For comparison, we plot the nine blue outliers of Komossa et al. (2008) with small black crosses. See the electronic edition of the Journal for a colour version of this figure.

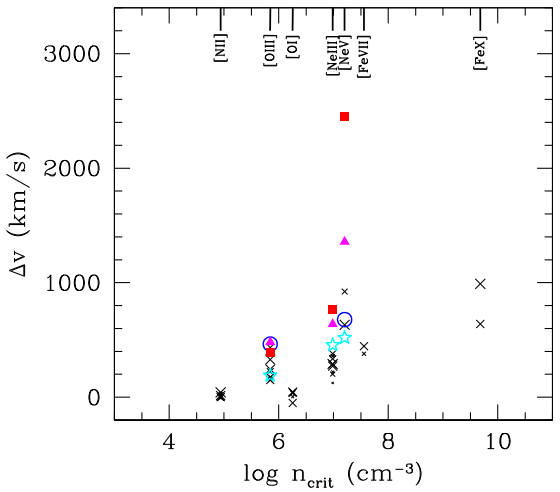

Figure 5. Radial velocity as a function of critical density $n_{\rm crit}$. The four galaxies of this study are marked by large red and blue symbols. For comparison, we plot the nine blue outliers of Komossa et al. (2008) with small black crosses. See the electronic edition of the Journal for a colour version of this figure.

In order to estimate Eddington ratios, $L_{\rm bol}/L_{\rm Edd}$, where the Eddington luminosity is given by

$$L_{\rm Edd} = 1.3\times10^{38}\frac{M_{\rm BH}}{M_\odot}\ {\rm erg\,s^{-1}}, \quad (2)$$

we utilize the close correlation between the luminosity of Hβ and the intrinsic continuum luminosity at 5100 Å. For NLS1 galaxies, Zhou et al. (2006) found that

$$\log(\lambda L_\lambda(5100\text{Å})) = 8.75 + 0.84\log {\rm L(H}\beta). \quad (3)$$

The bolometric luminosity then follows employing the relation of Kaspi et al. (2000), $L_{\rm bol} = 9\,\lambda L_\lambda(5100\ \text{Å})$. All radio-loud NLS1 galaxies of our sample accrete at high Eddington ratios (Table 3).

Alternatively, the Mg II-based virial SMBH masses were estimated, following Kong et al. (2006).

$$M_{\rm BH} = 10^{6.46}\left(\frac{L_{\rm Mg\,II}}{10^{42}\ {\rm erg\ s^{-1}}}\right)^{0.57}\left(\frac{\rm FWHM(H\beta)}{1000\,{\rm km s^{-1}}}\right)^2 {\rm M_\odot}. \quad (4)$$

These masses agree within better than a factor 2.6 with the Hβ-based masses (Table3).

2.10 Jet power

Radio data of the four NLS1 galaxies were collected from the literature (Table 1) and are based on non-simultaneous observations from the FIRST/NVSS survey at 1.4 GHz (Condon et al. 1998; Helfand et al. 2015), the GB survey at 4.85 GHz (Gregory & Condon 1991), data at 22 GHz (Doi et al. 2016), and observations at 151 MHz (Hales et al. 2007). The spectral index $\alpha_{\rm r}$ was calculated between 1.4 and 4.85 GHz, and defined as in $f_\nu \propto \nu^{\alpha_{\rm r}}$ (Table 1). Since for SDSSJ1634+4809 no measurement at 4.85 GHz is available, $\alpha_{\rm r} = 0$ was assumed. The intrinsic radio power νL_ν at rest-frame 1.4 GHz is given by

$$L_\nu = 4\pi r_{\rm l}^2 f_\nu (1+z)^{-1-\alpha_{\rm r}}, \quad (5)$$

where $\nu = 1.4$ GHz, $r_{\rm l}$ is the luminosity distance, and f_ν is the observed flux at 1.4 GHz (corresponding to a higher frequency in the source rest frame). We then use this number to perform an order of magnitude estimate for the jet power, $P_{\rm jet}$, following Birzan et al. (2008; their equation 16). Results are listed in Table 3. If the relation of Cavagnolo et al. (2010) is employed instead, higher values of $P_{\rm jet}$ are predicted by up to an order of magnitude. The jet Eddington ratio is defined as

$$\eta_{\rm jet} = P_{\rm jet}/L_{\rm Edd} \quad (6)$$

and given in Table 3.

3 NOTES ON INDIVIDUAL OBJECTS

SDSSJ1305+5116: This galaxy hosts the most massive SMBH in our mini sample (Table 3), at the very upper BH mass range observed for NLS1 galaxies (e.g. Xu et al. 2012). It shows the second highest outflow velocity in [Ne v]. 5 GHz VLBA radio images reveal a core–jet structure at parsec scales, and SDSSJ1305+5116 has one of the highest brightness temperatures of the NLS1 sample of Gu et al. (2015). At kpc scales, a second bright radio source is detected (Berton et al. 2018). Liao et al. (2015) reported evidence for a γ-ray flare from SDSSJ1305+5116.

SDSSJ1443+4725: It shows the highest outflow velocity, Δv([Ne v]) = 2450 km s^{-1} and is the strongest Fe II emitter, with R4570 = 2.2, in our sample. While the 1.4–4.85 GHz spectrum, based on non-simultaneous observations, is steep (Table 1), Berton et al. (2018) report a flat spectrum. On the other hand, the 5 GHz VLBA image is resolved into multiple components, all of them of steep spectrum (Gu et al. 2015). There is evidence for faint extended radio emission on kpc scales (Berton et al. 2018). A tentative γ-ray detection was presented by Liao et al. (2015).

SDSSJ1505+0326: It is the brightest radio source of our sample, and the radio loudest, with an inverted radio spectrum (Table 1), beamed and highly variably at radio frequencies (Angelakis et al. 2015; Lähteenmäki et al. 2017). It shows a compact core-jet structure on parsec scales (Dallacasa et al. 1998; D'Ammando et al. 2013), with mildly superluminal motion (1.1c ± 0.4c; Lister et al. 2016). SDSSJ1505+0326 was detected at γ-ray energies by the

Fermi satellite (Abdo et al. 2009b) including recent flaring activity (D'Ammando et al. 2016; Paliya & Stalin 2016). Applying BLR scaling relations, its Hβ-based virial black hole mass of 6.3×10^6 $M_\odot$ (Table 3) is relatively low given its high radio loudness. However, independent estimates show that the BH mass is still uncertain by a factor of a few, and perhaps more than an order of magnitude. Yuan et al. (2008) reported 4×10^6 $M_\odot$, while Berton et al. (2016) gave 1.8×10^7 $M_\odot$. Using Mg II, a virial BH mass of 1.0×10^7 $M_\odot$ was inferred (Table 3), while estimates from optical–UV spectral energy distribution (SED) models of the accretion disc emission range between 2×10^7 $M_\odot$ (Abdo et al. 2009b), 4.5×10^7 $M_\odot$ (Paliya & Stalin 2016), and 2×10^8 $M_\odot$ (Calderone et al. 2013), while D'Ammando et al. (2016) concluded that BH masses above few 10^7 $M_\odot$ are inconsistent with the UV SED. SDSSJ1505+0326 is mildly variable in the optical (Paliya et al. 2013) and IR (Jiang et al. 2012).

SDSSJ1634+4809: Its 5 GHz VLBA image shows only a compact core (Gu et al. 2015). Caccianiga et al. (2015) estimated a high star formation rate, but concluded that the radio emission is jet dominated. SDSSJ1634+4809 shows the smallest ionized gas velocities of our sample, with $\Delta v([\mathrm{Ne\,V}]) = 520\,\mathrm{km\,s^{-1}}$.

4 DISCUSSION

4.1 Mass of outflowing gas

It is interesting to perform an estimate of the mass of ionized gas which is involved in the outflow. As has become common for such type of estimates, it is assumed that 1/10 of the [O III] luminosity in the outflowing gas is associated with Hβ emission, consistent with estimates in Section 2.3. The Hβ luminosity is given by

$$L_{\mathrm{H}\beta} = \int\int j_{\mathrm{H}\beta} \mathrm{d}\Omega \mathrm{d}V, \tag{7}$$

where the gas emissivity

$$j_{\mathrm{H}\beta} = \frac{n^2}{4\pi}\, 1.24 \times 10^{-25}\,\mathrm{erg\,s^{-1}\,cm^{-3}\,ster^{-1}} \tag{8}$$

under case B recombination conditions and at $T = 10.000\,\mathrm{K}$ (Osterbrock 1989).

The mass of the outflowing gas is then given by

$$M_{\mathrm{out}} = 6.74 \times 10^7 \left(\frac{L_{\mathrm{H}\beta}}{10^{42}\,\mathrm{erg\,s^{-1}}}\right)\left(\frac{n}{100\,\mathrm{cm^{-3}}}\right)^{-1} \mathrm{M_\odot}, \tag{9}$$

where n is the gas density. In order to perform an estimate of the ionized gas mass in outflow, a gas density of $\log n = 2$ was used,[2] which then implies $M_{\mathrm{out}} = 0.9 \times 10^8$ $M_\odot$ for SDSSJ1305+5116, and values of $(0.3–1.6) \times 10^7$ $M_\odot$ for the other galaxies (Table 3). We finally note that the *ionized* gas component comprises only a small fraction of the total gas mass.

[2]While the gas in the NLR of AGN is composed of a range of densities (e.g. Komossa & Schulz 1997; Villar-Martin et al. 2016), a constant gas density of $\log n = 2$ is often adopted in similar work (e.g. Liu et al. 2013; Brusa et al. 2015; Husemann et al. 2016) for an order of magnitude estimate, and we follow the same approach here.

4.2 The driver of the outflow

4.2.1 Models and constraints from observations

The outflow velocities of the high-ionization emission-line gas measured here are remarkably large and similar to some of the highest velocities detected so far (e.g. Holt et al. 2003; Aoki, Kawaguchi & Ohta 2005; Nesvadba et al. 2011; Zakamska et al. 2016). The measured velocities of the high-ionization gas are above the escape velocity of the host galaxy.

What is the driving force of these flows? Radiation pressure acting on dust (e.g. Binette 1998; Dopita et al. 2002; Fabian, Celotti & Erlund 2006; Thompson et al. 2015) has been shown to be capable of accelerating dusty gas to significant velocities. Thermal winds need efficient acceleration (and deceleration) mechanisms, and have been employed to explain mild emission-line shifts in nearby Seyfert galaxies (e.g. Das et al. 2005). High radio luminosity is known to have an influence on the [O III] line width (Mullaney et al. 2013). Jet–cloud interactions are another possibility to drive local gas flows (e.g. Bicknell et al. 2000; Saxton et al. 2005; Wagner et al. 2012), including the possibility of entrainment of NLR clouds in the radio plasma of the jets. Clouds are prone to instabilities under these conditions (e.g. Blandford & Königl 1979; Schiano, Christiansen & Knerr 1995), but magnetic confinement has been suggested as a way out (Fedorenko, Paltani & Zentsova 1996). Accretion disc winds, seen in some cases as ultrafast outflows in X-rays up to ∼0.1c (Tombesi et al. 2012), may proceed into the inner NLR (Kurosawa & Proga 2008; Proga et al. 2008) and beyond, and may then shock and accelerate the NLR clouds and drive a large-scale outflow (Wagner et al. 2013; Cielo et al. 2018).

Here, we comment on the constraints on the different outflow scenarios, set by the reported observations.

4.2.1.1 Pole-on view. Orientation effects will contribute to increasing the observed radial velocities, if we have near pole-on views into the outflow cones, as expected for radio-loud, beamed sources. This will plausibly contribute to the higher fraction of blue outliers among radio-loud NLS1 galaxies (Yuan et al. 2008). At the same time, among the NLS1 galaxies of our mini-sample, the radio-loudest and strongly beamed source, SDSSJ1505+0326, does not show the highest outflow velocity, so that other factors must also play a role.

4.2.1.2 Cloud acceleration by radiation pressure. Recent simulations have shown that radiation pressure acting on dust can lead to high outflow velocities. IR photons which undergo multiple scattering events on dust in dense clouds efficiently transfer momentum to the gas, and this mechanism is capable of driving large-scale outflows with velocities up to 100–1000 $\mathrm{km\,s^{-1}}$ in luminous quasars (Bieri et al. 2017). Such a scenario would also explain, why the observed Balmer-line emitting BLR (in the NLS1 galaxies of our study) is not involved in the flow, since the flow would only be launched beyond the dust-survival radius. However, we do not find strong evidence for dust extinction in the optical spectra. First, the spectra are very blue. This still leaves the possibility of dust entrained with the narrow-line emitting gas, of which only a small fraction partially covers the continuum source. However, second, the observed ratio of [Ne V]/[O III] is very high, whereas strong extinction would significantly decrease [Ne V].

4.2.1.3 Fraction of matter-bounded clouds. While detailed photoionization modelling would be needed to understand all emission

line intensities, the high flux ratio of [Ne v]/[O iii] stands out. The average intensity ratio f_{Ne} of 0.54 of our mini-sample exceeds significantly the ratio observed in nearby Seyfert galaxies (Komossa & Schulz 1997) and the average of SDSS quasar spectra (f_{Ne} = 0.16; vanden Berk et al. 2001), and points to a higher-than-usual fraction of matter-bounded clouds in the NLR (e.g. Binette et al. 1997; Komossa & Schulz 1997), i.e. clouds of low column density with a higher degree of ionization, and which are more efficiently accelerated by jets or winds (Section 4.2.2).

4.2.1.4 Two-component NLR. The [O iii] emission line profile analysis has shown that there is little high-ionization gas at zero velocity. We therefore do not observe a two-component NLR in which a significant fraction of the NLR gas is at rest, while another NLR component is in outflow. Rather, a large fraction of the observed NLR participates in the outflow.[3] The observed ionization stratification points in the same direction.

4.2.1.5 Localized jet–cloud interactions of a narrow jet. We have inspected the dependence of radial velocity on ionization potential for all measured emission lines (Fig. 4). For comparison, the values measured for our previous sample of blue outliers are shown (K08), drawn from radio-quiet objects. The four galaxies follow the same pattern seen before. In particular, the higher ionization line [Ne v] which is also formed at higher critical density shows larger outflow velocity than the [O iii] emitting gas. This implies that either the [Ne v] emitting gas is more efficiently accelerated than the [O iii] emitting gas. Or else, that we see a large-scale outflow, which *decelerates* between the [Ne v] emission site further in, and the [O iii] emission site further out. These observations and the absence of a second, undisturbed NLR component argue against single, localized jet–cloud interactions.

4.2.1.6 Source youth/early blow-out phase. It is interesting to compare the phenomenon of blue outliers in NLS1 galaxies with that of outflows in radio galaxies, since both source types are likely in an early evolutionary stage. The phenomenon of emission-line shifts is also known among some young radio galaxies (e.g. Tadhunter et al. 2001; Holt et al. 2003, 2008; Marziani et al. 2003; Stockton et al. 2007; Nesvadba et al. 2008, 2011), and is often accompanied by significant outflows in the cold neutral gas (e.g. Morganti et al. 2010, 2013a,b; Mukherjee et al. 2018). These galaxies likely represent an early stage of radio-source evolution, where a joung jet interacts with a cocoon of dense gas in the central region. At least a fraction of these sources is likely triggered by mergers. The favoured mechanism for producing the line blueshifts is jet–cloud interactions in the inner NLR, and the blue outliers among the radio galaxies generally lack an ionization stratification (Holt et al. 2008), unlike the NLS1 galaxies, suggesting some difference in the evolutionary state, and/or the scale and driver of the outflows (we come back to a variant of this scenario in Section 4.2.2).

Since the radio-loud NLS1 galaxies of our sample show *both*, *near-Eddington accretion* likely associated with significant *outflows*, as well as powerful *radio jets*,[4] we next compare our salient results (especially high outflow velocities, strong [Ne v], higher line broadening for higher velocity shifts, presence of an ionization or density stratification) with state-of-the-art simulations of NLR-wide outflows, in order to assess under which conditions the observations can be best reproduced.

4.2.2 Implications from large-scale simulations of the interaction of disc winds and radio jets with NLR gas

Hydrodynamic simulations of jets and winds interacting with the ISM of the host galaxy give clues towards interpreting the data presented in this paper. Wagner & Bicknell (2011) and Wagner et al. (2012) performed relativistic hydrodynamic simulations of AGN jets interacting with a clumpy ISM on kpc scales, while Wagner et al. (2013) performed similar simulations for the case of disc winds. More recently, Bieri et al. (2017) performed radiation hydrodynamic simulations of galactic outflows driven mainly by the radiation pressure of infrared photons on dust.

These were all simulations of isolated galaxies modelled with idealized but realistic initial conditions employing a two-phase fractal ISM. The spatial resolution of the simulations was approximately 2 pc, allowing gas densities of up to a few 10^4 cm^{-3} to be sampled. The simulations were designed so that most of the AGN–ISM interactions occur on 1 kpc scales or less. The density inhomogeneities, dense cool clouds with temperatures between 30 and 30 000 K, in these simulations at small radii can therefore be associated with NLR clouds. The key to modelling realistic AGN outflows are the initial conditions of the inhomogeneous ISM. In all simulations, powerful multiphase gas outflows were generated by efficient momentum and energy transfer from the jet, or wind. The velocity dispersion and radial outflow velocities reached scale with AGN power and are sensitively dependent on the spatial distribution and mean column density of clouds. The higher the mean column densities, the harder it is to ablate and accelerate the clouds.

In the case of jets and winds, the jet or wind plasma percolates through the porous interstellar medium generating shear instabilities at the cloud interfaces, ablating and entraining the outer layer of clouds, and driving radiative shocks into the interior of the clouds. Clouds at all radii experience strong hydrodynamic ablation as well as core compression. The ablated cloud material was typically accelerated to 1000s km s^{-1}, while bulk clouds gained velocities of 100s km s^{-1} (e.g. Wagner & Bicknell 2011, their fig. 4). The momentum and energy transfer through jets and winds proceeds in a similar fashion, with jets exhibiting, on average, a somewhat larger momentum boost (mechanical advantage) and a stronger alignment signature, that is, material along the jet axis is more strongly accelerated and compressed than material far away from the jet axis (Wagner et al. 2016). On the whole, however, feedback by jets and winds is difficult to distinguish in terms of the kinematics of the dispersed gas. In fact, the kinematics of the dispersed gas is much more sensitive to its structure and spatial distribution at the time the SMBH becomes active.

[3] At the same time, the bulk of the low-ionization Hβ-emitting BLR is not part of this outflow, implying that either cloud acceleration occurs beyond the BLR scales, or else that only the high-ionization part of the BLR participates in the outflow as observed in quasars (review by Marziani et al. 2017).

[4] Since all our sources are very radio loud, this statement holds independent of a possible *beaming* correction. The estimate of radio power itself (our Section 2.10) is known to be uncertain, and we have therefore used the more conservative estimate [i.e. the one which predicts much lower radio powers (Section 2.10)]. Even if the radio powers reported in Table 3 were overestimated by a factor of 10, our salient conclusions would hold, in that they would still marginally be able to accelerate gas to the high observed velocities, if the NLR clouds are significantly fragmented (Wagner et al. 2012).

On kpc scales, AGN radiation on its own is less efficient than jets or fast winds in driving outflows (Cielo et al. 2018), but momentum boosts of tens of $L_{\rm bol}/c$ can be achieved through infrared photons trapped in dusty clouds, which provide most of the momentum boost (Bieri et al. 2017). Optical photons provide some momentum, and UV photons ionize and heat the outer layers of the clouds, but both are quickly reprocessed into infrared photons. Although shocks are driven into the clouds, photons penetrating the clouds rarify the gas within, rendering the clouds more diffuse than in the case of compression and acceleration by radio plasma.

The simplest explanation for the ionization stratification or density stratification (Section 2.7) is that one is observing a spatially correlated outflow that is decelerating with radius. This is in line with the trend in observations of nearby spatially resolved AGN that the [Ne v] emission is more compact than the [O iii] emission. Global deceleration of the outflow is seen in the later stages of the simulations with jets or winds, when the jet or wind plasma escapes the region covered by clouds and begins to blow a bubble beyond ∼1 kpc (see also Mukherjee et al. 2016). In the case of radiation-driven outflows, the coupling between radiation and gas diminishes and the outflow decelerates at later times (after a few Myr), because the efficiency with which outflows are accelerated depends primarily on the infrared optical depth, and the optical depth rapidly decreases with time as the gas is dispersed.

The deceleration in all cases is primarily through hydrodynamic drag. However, the deceleration seen in the simulations occurs globally and is mainly a function of time, rather than radius or density. Even at later times, the clouds at large radii and lower density generally have higher velocities than at smaller radii and larger densities. Note, however, that these simulations do not probe AGN–ISM interactions for much longer than a few Myr, and gas may couple differently with the jet, wind, and radiation when the dispersed clouds fall back in again through gravity. Furthermore, the simulations may not be resolving very small, fast-moving fragmented clouds at small radii, as the Jeans length is always only marginally resolved in these simulations.

Other deceleration mechanisms that are only marginally captured are (1) deceleration by gravity, which becomes important on scales exceeding a few kpc (i.e. beyond the baryonic scale radius; however, they are relatively unimportant for those galaxies of our sample with the highest velocities, well beyond the escape velocity) or on scales below a few tens of pc (i.e. the BH sphere of influence); and (2) deceleration by backflows. The latter is particularly relevant to jets and can, under certain circumstances, even influence gas flows down to parsec scales (Cielo et al. 2014).

Another possibility that may contribute to a density stratification is efficient radiative cooling of diffuse fast filaments of entrained gas. These filaments can exceed 1000 km s^{-1} well within 1 kpc, and in most of the simulations described above, the cooling time of the filaments is comparable to the dynamical time of the outflow over 1 kpc (e.g. Mukherjee et al. 2018). At small radii, ablation may be more efficient than contraction due to cooling, but, towards large radii, the accelerated filaments may condense, fragment, and collapse, experiencing reduced hydrodynamic drag and retaining much of the momentum they gained. The existence of fast dense gas at large radii may be consistent with the fact that (at least the low-ionization part of) the BLR does not appear to contribute to the outflow, but it may be at odds with the compact nature of [Ne v] (seen in many spatially resolved AGN, and reflecting the fact that the emission line requires a high-ionization parameter $U \propto Ln^{-1}r^{-2}$). If, however, this is the dominant reason for the density stratification, then such a stratification may imply feedback by jets or winds, rather than by radiation pressure for which radiative shocks and cooling are likely not as efficient. This effect is not well captured in simulations thus far, as numerical diffusion often dominates the realistic thermal history of the accelerated filaments. Global simulations would require higher levels of adaptive mesh refinement, but the fragmentation due to radiative cooling is seen in wind-tunnel simulations relevant to galactic outflows by Cooper et al. (2009) and Dugan et al. (2017).

Finally, a third possibility is that we are observing sources exhibiting ionization or density stratifications at early times in the evolution of the AGN outflow. In that case, denser clouds at smaller radii have experienced more acceleration than more diffuse clouds at larger radii, simply because the AGN bubble or the radiation has not had the time to influence the outer clouds much. In this case, however, we might expect a component of the NLR to be at rest, which is not seen in our sample – the entire NLR appears to be participating in the outflow. In the case of a jet that is still confined at smaller radii, the clouds at larger radii may be accelerated by the forward shock sweeping up the NLR and by secondary jet streams that propagate away from the main jet stream, percolating through the inter-cloud space all the way to the boundaries of the bubble. In general, this hypothesis requires that we are observing these AGN at a special time within a timeframe of < 1 Myr. Overall, this is consistent with other lines of evidence that NLS1 galaxies are young AGN in an early stage of their evolution (e.g. Mathur 2000a,b, Grupe 2004), and with the compactness of their radio emission (e.g. Komossa et al. 2006; Gu et al. 2015; Doi et al. 2016). None of the radio-loud galaxies of our sample shows large-scale radio emission (i.e. they are unrevolved by FIRST; Yuan et al. 2008), and the bulk of the radio emission arises on scales less than ∼200 pc (Gu et al. 2015). However, Berton et al. (2018) reported evidence for faint extended radio emission on kpc scales in SDSSJ1443+4725; SDSSJ1505+0326, and SDSSJ1634+4809, and the presence of a second bright radio source at 8 kpc separation in SDSSJ1305+5116. This is *very* compact when compared to the majority of radio-loud AGN, but is of the dimension of the NLR. Deeper radio observations at tens of kpc scales of our sample are needed to further constrain the dimensions of the radio emission at or beyond NLR scales.

In a recent comparison study between jet feedback and feedback by radiation pressure, Cielo et al. (2018) found that the phase space evolution at early times of radiation-driven outflows is different to that of jet-driven outflows. In the case of radiation-driven outflows, the inner regions of the clouds were accelerated first, followed by the more diffuse shadow regions, while in the case of jet- or wind-driven outflows, the outer regions of a cloud were first quickly ablated and accelerated, and the cloud cores were then accelerated in bulk by external pressure gradients. This leads to regions of positive correlation between outflow speed and density for up to ∼1 Myr in the case of radiation-driven outflows, while the correlation is already negative by then in the case of jet-driven outflows (Cielo et al. 2018, their fig. 6). The positive correlation in the former case disappears at later times.

In summary: (1) Our results are consistent with several key predictions from the simulations, in that the highest outflow velocities are reached in the two galaxies with the highest bolometric luminosities and jet powers (SDSSJ1305+5116 and SDSSJ1443+4725), there is evidence for a population of fragmented, matter-bounded clouds (high [Ne v]/[O iii] ratios) which are more efficiently accelerated to high velocities, and the small implied source lifetimes are in line with other evidence for the youth of NLS1 galaxies. (2) A well-defined ionization or density stratification remains more challenging to understand, but will provide tight constraints for

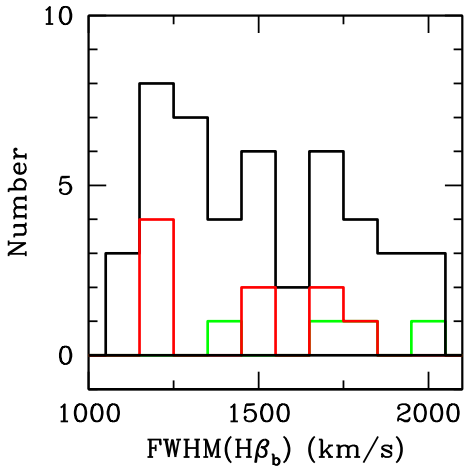

Figure 6. Histogram of the FWHM(H β) distribution of the sample of NLS1 galaxies of Xu et al. (2007). The histograms of the blue outliers of Komossa et al. (2008) and of the radio-loud NLS1 galaxies of this study are plotted for comparison, in red and green, respectively. Radio-loud NLS1 galaxies do not show systematically smaller line widths.

future models of mechanically driven feedback by jets or winds and feedback driven purely by radiation pressure, especially once global radiation-hydrodynamic simulations are coupled with non-equilibrium ionization calculations for all the observed species.

4.3 A note on orientation effects in NLS1 galaxies

While there is now several lines of evidence that the main driver of NLS1 activity and phenomenology is near- Eddington accretion onto low-mass black holes (e.g. Boroson 2002; Grupe et al. 2010; Xu et al. 2012), there is also circumstantial evidence that orientation plays a secondary role in affecting the observed properties of NLS1 galaxies (e.g. Collin et al. 2006). Ever since the identification of NLS1 galaxies as AGNs with the smallest widths of the broad Balmer lines, the question has been around, whether near face-on views onto flattened BLRs might contribute to the narrow width of the lines (e.g. Osterbrock & Pogge 1985).

In case of a heavily flattened BLR, the pole-on NLS1 galaxies (i.e. the beamed ones, and/or those with the strongest outflow components) should show a preference for more narrow Balmer lines. We have plotted in Fig. 6 the distribution of FWHM(H β) for a sample of 46 NLS1 galaxies (Xu et al. 2007; K08), excluding blue outliers. For comparison, the blue outliers of that sample (K08) are overplotted, as are the four NLS1 galaxies of the present study. Note that in order to make this comparison, we need to rely on alternative criteria for NLS1 classification, not using FWHM(H β). In fact, all NLS1 under study are still classified as such if we only use the ratio of [O III]/H β and the strength of Fe II as classification criterion. We find that the galaxies with the highest outflow velocities do not show a preference for the smallest Balmer lines, arguing against a highly flattened BLR in these sources. Since the sample size is small, this test has to be repeated with a larger number of sources.

5 SUMMARY AND CONCLUSIONS

The class of NLS1 galaxies is known to show, on average, higher [O III] outflow velocities than the class of BLS1 galaxies (e.g. K08). Even larger outflow velocities are found in the *radio-loud* NLS1 galaxies under study. These are therefore important laboratories for understanding large-scale, fast, outflows in AGN.

We find extreme outflow velocities (up to $\Delta v = 2450\,\mathrm{km\,s^{-1}}$) and highly broadened 'narrow' lines (up to FWHM $= 2270\,\mathrm{km\,s^{-1}}$) in four radio-loud NLS1 galaxies in [Ne V], and up to $\Delta v = 480\,\mathrm{km\,s^{-1}}$ in [O III].

It is the *whole* [O III] emission-line profiles which show these kinematic shifts. *Additional* blue wings in [O III] are also present, and are more highly shifted than the cores.

The highest ionization gas is above the escape velocity of the host galaxy.

The masses of the ionized gas in outflow are of the order of $(0.3\text{–}8.7) \times 10^7\,\mathrm{M_\odot}$.

The emission line width shows a very strong correlation with outflow velocity, so that the highest velocity gas component inevitably has very high velocity dispersion.

The presence of an ionization stratification (i.e. a correlation of outflow velocity with ionization potential), and the absence of significant zero-velocity high-ionization gas, disfavours single, localized jet–cloud interactions as the cause of the outflow. Rather, a large fraction of the NLR must be in outflow.

Comparison with hydrodynamic models of jets and winds interacting at NLR scales suggests that we may see NLS1s with high ionized-gas velocities in an early stage of their evolution, in a scenario where the denser, high-ionization clouds at smaller radii have experienced more acceleration than more diffuse clouds further out. In this scenario, the outer NLR has not yet been much affected by the jet per se, but the clouds may still be accelerated by the forward shock sweeping up the outer NLR, and by jet streams which propagate away from the main jet stream and percolate through the inter-cloud funnels. This scenario requires source lifetimes of typically < 1 Myr.

In addition, radio selection (especially beamed sources) might contribute to the high observed radial outflow velocities, since effects of polar outflows are more pronounced, if we have a near pole-on view into the central engine.

In summary, radio-loud Seyfert galaxies with extreme outflows are important test beds for driving mechanisms of large-scale, high-velocity outflows, for feedback processes in the relatively nearby Universe, and perhaps NLS1 orientation models.

ACKNOWLEDGEMENTS

DX acknowledges the support of the Chinese National Science Foundation (NSFC) under grant NSFC-11273027. AYW has been supported in part by ERC Project No. 267117 (DARK) hosted by Université Pierre et Marie Curie (UPMC) – Paris 6, PI J. Silk, and by the Australian Research Council through the Discovery Project, The Key Role of Black Holes in Galaxy Evolution, DP140103341. This research has made use of the SDSS data base and of the NASA/IPAC Extragalactic Database (NED) which is operated by the Jet Propulsion Laboratory, California Institute of Technology, under contract with the National Aeronautics and Space Administration. Funding for the SDSS and SDSS-II has been provided by the Alfred P. Sloan Foundation, the Participating Institutions, the National Science Foundation, the U.S. Department of Energy, the National Aeronautics and Space Administration, the Japanese Monbukagakusho, the Max Planck Society, and the Higher Education Funding Council for England. The SDSS Web Site is http://www.sdss.org/. The SDSS is managed by the Astrophysical Research Consortium for the Participating Institutions. The Participating Institutions are the American Museum of Natural History, Astrophysical Institute Potsdam, Uni-

versity of Basel, University of Cambridge, Case Western Reserve University, University of Chicago, Drexel University, Fermilab, the Institute for Advanced Study, the Japan Participation Group, Johns Hopkins University, the Joint Institute for Nuclear Astrophysics, the Kavli Institute for Particle Astrophysics and Cosmology, the Korean Scientist Group, the Chinese Academy of Sciences (LAMOST), Los Alamos National Laboratory, the Max-Planck-Institute for Astronomy (MPIA), the Max-Planck-Institute for Astrophysics (MPA), New Mexico State University, Ohio State University, University of Pittsburgh, University of Portsmouth, Princeton University, the United States Naval Observatory, and the University of Washington.

REFERENCES

Abazajian K. N. et al., 2009, ApJS, 182, 543
Abdo A. A. et al., 2009a, ApJ, 699, 976
Abdo A. A. et al., 2009b, ApJ, 707, L142
Abdo A. A. et al., 2009c, ApJ, 707, 727
Angelakis E. et al., 2015, A&A, 575, 55
Aoki K., Kawaguchi T., Ohta K., 2005, ApJ, 618, 601
Bae H.-J., Woo J.-H., 2014, ApJ, 795, 30
Bae H.-J., Woo J.-H., 2016, ApJ, 828, 97
Berton M., Foschini L., Ciroi S, Cracco V., La Mura G., Di Mille F., Rafanelli P., 2016, A&A, 591, A88
Berton M. et al., 2018, preprint (arXiv:180103519B)
Bicknell G. V., Sutherland R. S., van Breugel W. J. M., Dopita M. A., Dey A., Miley G. K., 2000, ApJ, 540, 678
Bieri R., Dubois Y., Rosdahl J., Wagner A., Silk J., Mamon G. A., 2017, MNRAS, 464, 1854
Binette L., 1998, MNRAS, 294, L47
Binette L., Wilson A. S., Raga A., Storchi-Bergmann T., 1997, A&A, 327, 909
Birzan L., McNamara B. R., Nulsen P. E. J., Carilli C. L., Wise M. W., 2008, ApJ, 686, 859
Blandford R., Königl A., 1979, ApL, 20, 15
Boroson T. A., 2002, ApJ, 565, 78
Boroson T. A., 2005, ApJ, 130, 381
Bruhweiler F., Verner E., 2008, ApJ, 675, 83
Brusa M. et al., 2015, MNRAS, 446, 2394
Caccianiga A. et al., 2015, MNRAS, 451, 1795
Calderone G. et al., 2013, MNRAS, 431, 210
Capetti A., Axon D. J., Macchetto F. D., Marconi A., Winge C., 1999, ApJ, 516, 187
Cavagnolo K. W., McNamara B. R., Nulsen P. E. J., Carilli C. L., Jones C., Bîrzan L., 2010, ApJ, 720, 1066
Churazov E., Brüggen M., Kaiser C. R., Böhringer H., Forman W., 2001, ApJ, 554, 261
Cielo S., Antonuccio-Delogu V., Macciò A. V., Romeo A. D., Silk J., 2014, MNRAS, 439, 2903,
Cielo S., Bieri R., Volonteri M., Wagner A. Y., Dubois Y., 2018, preprint (arXiv:171203955C)
Colbert E. J. M., Baum S. A., Gallimore J. F., O'Dea C. P., Lehnert M. D., Tsvetanov Z. I., Mulchaey J. S., Caganoff S., 1996, ApJS, 105, 75
Collin S., Kawaguchi T., Peterson B. M., Vestergaard M., 2006, A&A, 456, 75
Condon J. J., Cotton W. D., Greisen E. W., Yin Q. F., Perley R. A., Taylor G. B., Broderick J. J., 1998, AJ, 115, 1693
Cooper J. L., Bicknell G. V., Sutherland R. S., Bland-Hawthorn J., 2009, ApJ, 703, 330
Costa T., Rosdahl J., Sijacki D., Haehnelt M. G., 2018, MNRAS, 473, 4197
Cracco V., Ciroi S., Berton M., Di Mille F., Foschini L., La Mura G., Rafanelli P., 2016, MNRAS, 462, 1256
Crenshaw D. M., Kraemer S. B., 2007, ASP Conf. Ser., 373, 319
D'Ammando F. et al., 2012, MNRAS, 426, 317
D'Ammando F. et al., 2013, MNRAS, 433, 952
D'Ammando F., Orienti M., Larsson J., Giroletti M., 2015, MNRAS, 452, 520
D'Ammando F. et al., 2016, MNRAS, 463, 4469
Dallacasa D., Bondi M., Alef W., Mantovani F., 1998, A&AS, 129, 219
Das V. et al., 2005, AJ, 130, 945
Das V., Crenshaw D. M., Kraemer S. B., Deo R. P., 2006, AJ, 132, 620
De Robertis M. M., Osterbrock D. E., 1984, ApJ, 286, 171
di Matteo T., Springel V., Hernquist L., 2005, Nature, 433, 604
Doi A., Oyama T., Kono Y., Yamauchi A., Suzuki S., Matsumoto N., Tazaki F., 2016, PASJ, 68, 73
Dopita M., Groves B. A., Sutherland R. S., Binette L., Cecil G., 2002, ApJ, 572, 753
Dugan Z., Gaibler V., Bieri R., Silk J., Rahman M., 2017, ApJ, 839, 103
Elvis M., 2006, MemSAIt, 77, 573
Fabian A., 1999, MNRAS, 308, L39
Fabian A., 2012, ARAA, 50, 455
Fabian A., Celotti A., Erlund M. C., 2006, MNRAS, 373, L16
Fedorenko V. N., Paltani S., Zentsova A. S., 1996, A&A, 314, 368
Foschini L., 2011, Proc. Sci., Narrow-Line Seyfert 1 Galaxies and Their Place in the Universe. PoS(NLS1)024
Goodrich R. W., 1989, ApJ, 342, 224
Gregory P. C., Condon J. J., 1991, ApJS, 75, 1011
Grupe D., 2004, AJ, 127, 1799
Grupe D., Komossa S., Leighly K. M., Page K. L., 2010, ApJS, 187, 64
Gu M., Chen Y., Komossa S., Yuan W., Shen Z., Wajima K., Zhou H., Zensus J. A., 2015, ApJS, 221, 3
Hales S. E. G., Riley J. M., Waldram E. M., Warner P. J., Baldwin J. E., 2007, MNRAS, 382, 1639
Harrison C. M., Alexander D. M., Mullaney J. R., Swinbank A. M., 2014, MNRAS, 441, 3306
Helfand D. J., White R. L., Becker R. H., 2015, ApJ, 801, 26
Holt J., Tadhunter C. N., Morganti R., 2003, MNRAS, 342, 227
Holt J., Tadhunter C. N., Morganti R., 2008, MNRAS, 387, 639
Hopkins P., Elvis M., 2010, MNRAS, 401, 7
Hopkins P., Torrey P., Faucher-Giguère C.-A., Quataert E., Murray N., 2016, MNRAS, 458, 816
Husemann B., Scharwächter J., Bennert V. N., Mainieri V., Woo J.-H., Kakkad D., 2016, A&A, 594, A44
Jiang N. et al., 2012, ApJ, 759, 31
Jin C., Ward M., Done C., 2012, MNRAS, 422, 3268
Kaspi S., Smith P. S., Netzer H., Maoz D., Jannuzi B. T., Giveon U., 2000, ApJ, 533, 631
Kellermann K. I., Sramek R., Schmidt M., Shaffer D. B., Green R., 1989, AJ, 98, 1195
Komossa S., Schulz H., 1997, A&A, 323, 31
Komossa S., Xu D., 2007, ApJ, 667, L33
Komossa S., Voges W., Xu D, Mathur S., Adorf H-M., Lemson G., Duschl W. J., Grupe D., 2006, AJ, 132, 531
Komossa S., Xu D., Zhou H., Storchi-Bergmann T., Binette L., 2008, ApJ, 680, 926 (K08)
Komossa S. et al., 2015, A&A, 574, A121
Komossa S., Xu D., Zensus J. A., 2016, IAU Symp., 312, 36
Kong M.-Z., Wu X.-B., Wang R., Han J.-L., 2006, Chin. J. Astron. Astrophys., 6, 396
Kraemer S., Crenshaw M., 2000, ApJ, 532, 256
Kraemer S., Trippe M. L., Crenshaw D. M., Meléndez M., Schmitt H. R., Fischer T. C. 2009, ApJ, 698, 106
Kriss G. A., 1994, in Crabtree D. R., Hanisch R. J., Barnes J., eds., ASP Conf. Ser. Vol. 61, Astronomical Data Analysis Software and Systems III. Astron. Soc. Pac., San Francisco , p. 437
Kurosawa R., Proga D., 2008, ApJ, 674, 97
Lähteenmäki A. et al., 2017, A&A, 603, A100
Liao N. H., Liang Y. F., Weng S.-S., Berton M., Gu M.-F., Fan Y. Z., 2015, preprint (arXiv:151005584L)
Lister M. et al., 2016, AJ, 152, 12
Liu G., Zakamska N. L., Greene J. E., Nesvadba N. P. H., Liu X., 2013, MNRAS, 436, 2576

Marziani P., Zamanov R. K., Sulentic J. W., Calvani M., 2003, MNRAS, 345, 1133
Marziani P., Sulentic J. W., Stirpe G. M., Dultzin D., Del Olmo A., Martínez-Carballo M. A., 2016, Ap&SS, 361, 3
Marziani P., Negrete C. A., Dultzin D., Martínez-Aldama M. L., Del Olmo A., D'Onofrio M, Stirpe G. M., 2017, Frontiers Astron. Space Sci., 4, 16
Mathur S., 2000a, New Astron. Rev., 44, 469
Mathur S., 2000b, MNRAS, 314, L17
Mazzalay X., Rodríguez-Ardila A., Komossa S., 2010, MNRAS, 405, 1315
Moll R. et al., 2007, A&A, 463, 513
Morganti R., Holt J., Tadhunter C., Oosterloo T., 2010, IAU Symp., 267, 429
Morganti R., Frieswijk W., Oonk R. J. B., Oosterloo T., Tadhunter C., 2013a, A&A, 552, L4
Morganti R., Fogasy J., Paragi Z., Oosterloo T., Orienti M., 2013b, Science, 341, 1082
Mukherjee D., Bicknell G. V., Sutherland R., Wagner A., 2016, MNRAS, 461, 967
Mukherjee D., Wagner A. Y., Bicknell G. V., Morganti R., Osterloo T., Nesvadba N., Sutherland R. S., 2018, MNRAS, 476, 80
Mullaney J. R., Alexander D. M., Fine S., Goulding A. D., Harrison C. M., Hickox R. C., 2013, MNRAS, 433, 622
Murray N., Chiang J., Grossman S. A., Voit G. M, 1995, ApJ, 451, 498
Nesvadba N., Lehnert M. D., De Breuck C., Gilbert A. M., van Breugel W., 2008, A&A, 491, 407
Nesvadba N., Polletta M., Lehnert M. D., Bergeron J., De Breuck C., Lagache G., Omont A., 2011, MNRAS, 415, 2359
Osterbrock D. E., 1989, Astrophysics of Gaseous Nebulae and Active Galactic Nuclei, University Science Books, Mill Valley, CA
Osterbrock D. E., Pogge R., 1985, ApJ, 297, 166
Paliya V. S., Stalin C. S., 2016, ApJ, 820, 52
Paliya V. S., Stalin C. S., Kumar B., Kumar B., Bhatt V. K., Pandey S. B., Yadav R. K. S., 2013, MNRAS, 428, 2450
Paliya V. S., Ajello M., Rakshit S., Mandal A. K., Stalin C. S., Kaur A., Hartmann D., 2018, ApJ, 853, L2
Penston M. V., Fosbury R. A. E., Boksenberg A., Ward M. J., Wilson A. S., 1984, MNRAS, 208, 347
Perna M., Lanzuisi G., Brusa M., Mignoli M., Cresci G. , 2017, A&A, 603, 99
Proga D., Stone J. M., Kallman T. R., 2000, ApJ, 543, 686
Proga D., Ostriker J. P., Kurosawa R., 2008, ApJ, 676, 101
Rakshit S., Stalin C. S., Chand H., Zhang X.-G., 2017, ApJS, 229, 39
Rupke D. S. N., Gültekin K., Veilleux S., 2017, ApJ, 850, 40
Saxton C. J., Bicknell G. V., Sutherland R. S., Midgley S., 2005, MNRAS, 359, 781
Schiano A. V. R., Christiansen W. A., Knerr J. M., 1995, ApJ, 439, 237
Schlegel D. J., Finkbeiner D. P., Davis M. 1998, ApJ, 500, 525
Schneider D. P. et al., 2007, AJ, 134, 102
Shen Y., 2016, ApJ, 817, 55
Shen Y. et al., 2011, ApJS, 194, 45
Springel V., Di Matteo T., Hernquist L., 2005, ApJ, 620, L79
Stockton A., Canalizo G., Fu H., Keel W., 2007, ApJ, 659, 195
Sulentic J., Marziani P., Zamanov R., Bachev R., Calvani M., Dultzin-Hacyan D., 2002, ApJ, 566, L71
Tadhunter C., Wills K., Morganti R., Oosterloo T., Dickson R., 2001, MNRAS, 327, 227
Thompson T. A., Fabian A. C., Quataert E., Murray N., 2015, MNRAS, 449, 147
Tombesi F., Cappi M., Reeves J. N., Braito V., 2012, MNRAS, 422, L1
vanden Berk D. E. et al., 2001, AJ, 122, 549
Véron-Cetty M. P., Véron P., Goncalves A. C., 2001, A&A, 372, 730
Véron-Cetty M. P., Joly M., Véron P., 2004, A&A, 417, 515
Vestergaard M., Peterson B. M., 2006, ApJ, 641, 689
Villar-Martin M., Humphrey A., Delgado R. G., Colina L., Arribas S., 2011, MNRAS, 418, 2032
Villar-Martin M., Arribas S., Emonts B., Humphrey A., Tadhunter C., Bessiere P., Cabrera Lavers A., Ramos Almeida C., 2016, MNRAS, 460, 130
Wagner A. Y., Bicknell G. V., 2011, ApJ, 728, 29
Wagner A. Y., Bicknell G. V., Umemura M., 2012, ApJ, 757, 136
Wagner A. Y., Umemura M., Bicknell G. V., 2013, ApJ, 763, L18
Wagner A. Y., Bicknell G. V., Umemura M., Sutherland R. S., Silk J., 2016, Astron. Nachr., 337, 167
Wang J., Xu D. W., Wei J. Y., 2018, ApJ, 852, 26
Woo J.-H., Bae H.-J., Son D., Karouzos M., 2016, ApJ, 817, 108
Wright E. L., 2006, PASP, 118, 1711
Wyithe J. S. B., Loeb A., 2003, ApJ, 595, 614
Xu D., Komossa S., Zhou H., Wang T., Wei J., 2007, ApJ, 670, 60
Xu D., Komossa S., Zhou H., Lu H., Li C., Grupe D., Wang J., Yuan W., 2012, AJ, 143, 83
Yang H. et al., 2018, MNRAS, in press (arXiv:1801.03963)
Yao S., Yuan W., Zhou H., Komossa S., Zhang J., Qiao E., Liu B., 2015, MNRAS, 454, L16
York D. G. et al., 2000, AJ, 120, 1579
Yuan W., Zhou H. Y., Komossa S., Dong X. B., Wang T. G., Lu H. L., Bai J. M., 2008, ApJ, 685, 801
Zakamska N. L. et al., 2016, MNRAS, 459, 3144
Zamanov R., Marziani P., Sulentic J. W., Calvani M., Dultzin-Hacyan D., Bachev R., 2002, ApJ, 576, L9
Zhang K., Dong X.-B., Wang T.-G., Gaskell C. M., 2011, ApJ, 737, 71
Zhou H.-Y., Wang T., Yuan W., Lu H., Dong X., Wang J., Lu Y., 2006, ApJS, 166, 128
Zubovas K., King A., 2012, ApJ, 745, L34

This paper has been typeset from a TEX/LATEX file prepared by the author.